Camelid single-domain antibodies: A versatile tool for in vivo imaging of extracellular and intracellular brain targets

Tengfei Li, Matthias Vandesquille, Fani Koukouli, Clémence Dudeffant, Ihsen Youssef, Pascal Lenormand, Christelle Ganneau, Uwe Maskos, Christian Czech, Fiona Grueninger, et al.

HAL Id: pasteur-01375692

https://pasteur.hal.science/pasteur-01375692

Submitted on 3 Oct 2016

Camelid single-domain antibodies:
A versatile tool for *in vivo* imaging of extracellular and intracellular brain targets

Tengfei Li [a,b,c,1] , **Matthias Vandesquille** [d,e,f,g,1] , **Fani Koukouli** [h] , **Clémence Dudeffant** [b,f,g] , **Ihsen Youssef** [b] , **Pascal Lenormand** [a] , **Christelle Ganneau** [d,e] , **Uwe Maskos** [h] , **Christian Czech** [i] , **Fiona Grueninger** [i] , **Charles Duyckaerts** [b] , **Marc Dhenain** [f,g] , **Sylvie Bay** [d,e] , **Benoît Delatour** [b] , **Pierre Lafaye** [a,*]

[a] Institut Pasteur, CITECH, Plateforme d'Ingénierie des Anticorps, 75724 Paris Cedex 15, France.
[b] Sorbonne Universités, UPMC Univ. Paris 06 UMR S 1127, and Inserm, U 1127, and CNRS UMR 7225, and ICM, F-75013, Paris, France.
[c] Université Paris Descartes, Paris 5, France .
[d] Institut Pasteur, Unité de Chimie des Biomolécules, 75724 Paris Cedex 15, France.
[e] CNRS UMR 3523, 75724 Paris Cedex 15, France.
[f] Commissariat à l'Energie Atomique et aux Energies Alternatives (CEA), Direction de la Recherche Fondamentale (DRF), Institut d'Imagerie Biomédicale (I2BM), MIRCen, F-92260 Fontenay-aux-Roses, France.
[g] Centre National de la Recherche Scientifique (CNRS), Université Paris-Sud, Université Paris-Saclay UMR 9199, Neurodegenerative Diseases Laboratory, F-92260 Fontenay-aux-Roses, France.
[h] Institut Pasteur, Neurobiologie intégrative des systèmes cholinergiques, CNRS UMR 3571, Paris, France.
[i] F. Hoffmann-La Roche AG, Pharmaceutical Research and Early Development, NORD DTA, Roche Innovation Center Basel, CH-4070 Basel, Switzerland.
[1] Authors contributed equally to this work.

*Corresponding author. E-mail address: pierre.lafaye@pasteur.fr

ABSTRACT

Detection of intracerebral targets with imaging probes is challenging due to the non-permissive nature of blood-brain barrier (BBB). The present work describes two novel single-domain antibodies (VHHs or nanobodies) that specifically recognize extracellular amyloid deposits and intracellular tau neurofibrillary tangles, the two core lesions of Alzheimer's disease (AD). Following intravenous administration in transgenic mouse models of AD, *in vivo* real-time two-photon microscopy showed gradual extravasation of the VHHs across the BBB, diffusion in the parenchyma and labeling of amyloid deposits and neurofibrillary tangles. Our results demonstrate that VHHs can be used as specific BBB-permeable probes for both extracellular and intracellular brain targets and suggest new avenues for therapeutic and diagnostic applications in neurology.

1. Introduction

Brain penetration of targeted compounds, such as high affinity antibodies, is a prerequisite for the treatment and diagnosis of central nervous system pathologies. However, the entry into the central nervous system of most of blood-circulating molecules is seriously limited by the blood-brain barrier (BBB). It has been shown that only 0.02% - 0.1% of conventional immunoglobulins present in serum can penetrate into brain parenchyma [1,2]. Hijacking the BBB receptor-mediated transcytosis system has been envisioned as a way of promoting passage of agents in the brain. Antibodies directed against the transferrin receptor [3], or the insulin receptor [4] have hence been used as Trojan horses to transport therapeutic molecules across the BBB. Unfortunately, receptor-mediated transcytosis targets are highly and broadly expressed in tissues and are often implicated in critical cellular functions, therefore raising possible safety risks [5,6]. Artificial BBB opening by ultrasound [7,8] or by means of BBB permeability enhancers (*e.g.* mannitol [9]) is also an option to facilitate the penetration of compounds within the brain but these methods also have safety limitations [10].

Another approach of targeting intracerebral epitopes relies on the use of homodimeric heavy chain-only antibodies naturally produced in camelidae [11]. These "non-conventional" single-domain antibodies are devoid of light chains and their heavy chain variable domain (VHH) acts as a fully functional binding moiety [12]. VHHs have several unique features such as relatively low molecular weight, high production yield, high stability and solubility with the ability to specifically bind target epitopes at subnanomolar affinity. Due to their small size (15 kDa), VHHs occupy only 1/10 of the volume filled by conventional antibodies [11]. Consequently, they can diffuse more rapidly and deeply in fixed tissues [13] and have a better biodistribution profile *in vivo* than conventional antibody fragments [14,15]. Depending on their binding properties, VHHs can be used either to visualize and/or to interact with intracellular targets [16–22].

We recently demonstrated that some VHHs with a basic isoelectric point (pI) are able to readily transmigrate across the BBB *in vivo* after peripheral injection, without the need of any invasive or hazardous procedures (such as opening of the barrier using chemical or ultrasound sonication) [18]. These VHHs can be used as specific transporters as demonstrated by *in vivo* labeling of astrocytes with a VHH-fluorophore conjugate targeting the intracellular protein GFAP [18].

In the present work we engineered two new VHHs that were able to detect extracellular or intracellular pathological brain targets, namely the two main neuropathological lesions in Alzheimer's disease (amyloid plaques and neurofibrillary tangles - NFTs). We designed sensitive and specific anti-Aβ and anti-tau VHHs that allowed detection of plaques and NFTs in brain tissue from patients with Alzheimer's disease and from mouse models of the disease. We also showed that plaques and tangles could be visualized *in vivo* in mice following intravenous administration of these probes.

2. Materials and methods

The main experimental procedures are described here. Detailed materials and methods are provided in Supplementary Materials.

2.1. Human AD brain extracts and immunization

A male alpaca was immunized with 1mg of fibrillar synthetic Aβ 42 peptide (Bachem). One alpaca was immunized with tangles-enriched AD extracts (Braak stage V and VI) that were obtained from the NeuroCEB brain bank. This bank is associated to a brain donation program run by a consortium of patient associations (including France Alzheimer Association) and declared to the Ministry of Research and Universities, as requested by French Law. An explicit written consent was obtained for the brain donation in accordance with the French Bioethical Laws. Another alpaca was immunized with a synthetic mono-phosphorylated peptide derived from the C-terminus of the tau protein. A detailed description is provided in Supplementary Materials.

2.2. Library construction, phage preparation and phage display

The library construction was described in [23]. Phages were prepared by transformation of *E.coli* host cells with a recombinant phagemid and a helper phage. A large number of phages (10^{13}) and different blocking buffers were used to perform each round of phage-display. A complete description is provided in Supplementary Materials.

2.3. Selection of specific phage-VHHs and binding epitope determination of monoclonal phage-VHH

The libraries of anti-Aβ and anti-pTau VHHs were panned for reactivity with biotinylated Aβ42, Aβ40 peptides and full-length pTau protein respectively. Epitope mapping of Aβ specific VHHs was performed by the ELISA inhibition test. A detailed protocol is provided in Supplementary Materials.

2.4. Expression of VHHs

The coding sequences of the selected VHHs (R3VQ and A2) in the vector pHEN1 were sub-cloned into a bacterial expression vector pET23d (Novagen) containing a 6-Histidine tag using NcoI and NotI restriction sites. Purified VHHs were isolated from transformed *E. coli* BL21 (DE3) pLysS cells by immobilized-metal affinity chromatography (IMAC). The full method is described in Supplementary Materials.

2.5. Determination of pI by IsoElectric Focusing (IEF)

The pI of VHHs was determined by isoelectric focusing using IEF 3-10 Gel (Invitrogen). NEPGHE (non equilibrium pH gradient gel electrophoresis) with sample application at the anode was also used because it allows optimal protein analysis in the basic range of the gel including pI 8.5 to 10.5 (SERVA Gel IEF 3-10 instruction manual).

2.6. Preparation of AlexaFluor 488-conjugated VHH and mAb

The cysteine present in the C-terminal region of VHH and the SH group in the hinge region of reference mAbs (4G8 and muRb86) were used to realize the conjugation with the maleimido-AF488 fluorophore (Invitrogen). A detailed description is provided in Supplementary Materials.

2.7. Animal models

PS2APP mice overexpressing hAPP Swedish mutation combined with PS2 N141I mutation [24,25] were used as animal models harboring Aβ-positive lesions. PS2APP mice start to develop overt Aβ deposition in the brain at approximately 6 months of age.

Tg4510 mice with the hMAPT P301L gene mutation [26] were used as NFT-bearing mouse model. NFT start to appear in the cortex by 4 months of age and one month later in the hippocampus. All animal experiments were performed in accordance with the guidelines established by European Union legislation regarding the use and care of laboratory animals. Four PIs of the present study (B. D., Pi.L., M.V. and M.D.) have received official agreements from the French Ministry of Agriculture to carry out research and experiments on animals.

2.8. Stereotaxic injections of VHHs

Stereotaxic injections of each VHH were performed in anesthetized mice. Two microliters of VHH was injected into the frontal cortex at the rate of 0.2µl /min. Two or 24 hours later, brains were collected for histological analysis. A detailed protocol is provided in Supplementary Materials.

2.9. Immunohistochemistry and double immunofluorescence staining

Immunohistochemistry was primarily performed on 4µm thick paraffin sections. A pre-treatment with formic acid was performed before neutralization of endogenous peroxidase activity. After incubation with primary and secondary antibodies (see Supplementary Materials), standard immuno-peroxydase method was applied with DAB as final chromogen. Immunohistochemistry on free-floating sections, fresh tissues and VHH-exposed tissues was performed with similar procedures. Double immunofluorescence staining was implemented on paraffin sections using standard protocols. A detailed description is provided in Supplementary Materials.

2.10. Estimation of lesion loads by VHHs and reference antibodies

Comparative lesion loads detected by VHHs vs reference antibodies were assessed on immunostained sections obtained from PS2APP and Tg4510 mice. The full method is described in Supplementary Materials.

2.11. Intravenous administration of AF488-conjugated VHH and monoclonal antibodies

AlexaFluor conjugated VHH was slowly injected into the caudal vein of the AD mice. Two-photon imaging was then performed during the 2-4 subsequent hours. For control experiments relying on peripheral injections with no *in vivo* imaging, the same procedures were applied but no cranial surgery was performed. A detailed protocol is provided in Supplementary Materials.

2.12. *In vivo two-photon imaging*

Mice were anesthetized. Their head was immobilized and a small craniotomy was performed above the right hemisphere. A detailed description of the craniotomy surgery is provided in Supplementary Materials. Two-photon imaging was performed with a two-photon laser-

scanning microscope system and PrairieView software (Prairie Technologies, Middelton, WI), using a 16x 0.8 NA water immersion objective (Nikon, Tokyo, Japan) with the two-photon laser tuned to 920 nm (MaiTai DeepSee, Spectra Physics, Mountain View, CA). The images were acquired at 512 x 512 with a pixel size of 0.5 um. Care was taken to use less than 20 mW of laser power in the tissue. The raw data obtained were processed using Image J software for analysis and 3D rendering.

3. RESULTS

3.1. Selection and characterization of a VHH recognizing extracellular targets

3.1.1. Generation and optimization of R3VQ

One alpaca was immunized with a fibrillar synthetic Aβ42 peptide and a specific VHH library was constructed from cDNA encoding VHH domains isolated from lymphocytes. The total size of the library contained 1x 10^8 phage-VHHs. VHHs were selected by Phage Display through 3 panning cycles with biotinylated Aβ42 and Aβ40 peptides at different concentrations of antigens, buffer and washing conditions. Four hundreds individual clones were tested by ELISA using biotinylated Aβ42. Two VHHs were obtained, called R3VQ and R3VE respectively. They differed by only one amino acid: a glutamine (Q) of R3VQ was replaced by a glutamic acid (E) in R3VE. R3VQ recognized an epitope located in the central part of the Aβ peptide between aa 17-28 (Fig. S1A).

C terminal His tagged VHH R3VQ and R3VE were obtained after subcloning of their genes in pET23d vector. Both VHHs had high production yields about 20 and 9mg/l of culture, respectively. Note that in the present study, R3VQ and R3VE represent R3VQ-His and R3VE-His antibodies unless otherwise mentioned. As a basic pI favors BBB passage [18], we decided to focus our study on R3VQ, which had a higher pI than R3VE (see below). R3VQ showed good purity with only one band observed by SDS-PAGE (Fig. 1A). It had a basic pI > 8.3 (Fig. 1B). By ELISA, R3VQ showed strong binding to Aβ40 and Aβ42 (Fig. 1C).
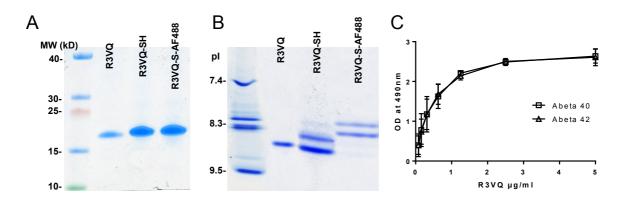

Fig. 1. Biochemical characterization of R3VQ and its variants.

(A) Analysis of R3VQ variants by SDS-PAGE. (B) Determination of pI of R3VQ variants by NEPHGE on 3-10 IEF gel. (C) Binding of purified R3VQ to biotinylated Aβ40 and 42 determined by ELISA.

We engineered a fluorescent conjugate to allow *in vivo* imaging with microscopic resolution. For this purpose, an additional cysteine residue was inserted in the C terminal part of the sequence of R3VQ (referred as R3VQ-SH), thus allowing a C terminal thio-addition of a maleimido-Alexa fluor dye (AF488) by a site specific approach [27]. The coding sequence of R3VQ-SH contained a N-terminal 6-histidine tag for purification and detection.

In this way we obtained a well-defined conjugate with only one AF488 molecule (Fig. 1A). This final compound was referred to as R3VQ-S-AF488. The pI of R3VQ-SH and R3VQ-S-AF488 were analyzed by NEPHGE using IEF 3-10 gel. The pI of R3VQ-SH was between 8.3 and 9.5 (Fig. 1B), similar to that of R3VQ. The addition of maleimido-AF488 to R3VQ-SH decreased its pI to ca. 8.3 (Fig. 1B). The two bands on IEF gel indicate the presence of two isoforms for both R3VQ-SH and R3VQ-S-AF488.

3.1.2. Immunodetection of Aβ brain lesions in mice and in human brain sections

VHH immunohistochemistry (IHC) was performed in plaques-enriched AD tissues (isocortical samples) and in PS2APP mice [24,25] harboring amyloid deposits. R3VQ showed excellent sensitivity and selectivity in detecting extracellular amyloid plaques and cerebral amyloid angiopathy (CAA), both on human and mouse paraffin sections pre-treated with formic acid [28] (Fig. 2A-B). Immunodetection of amyloid plaques was also possible on fresh brain tissues from AD patients without the use of any antigen retrieval pre-treatement (Fig. S1B). Double labeling performed on mouse sections using 4G8 (as a gold-standard anti-Aβ monoclonal antibody (mAb)) and R3VQ showed a very good colocalization of the two antibodies (Fig. 2C). Comparison of amyloid loads detected by R3VQ and 4G8 showed excellent correlation between the results obtained with the two antibodies (Fig. S1C). No labeling was observed following R3VQ IHC on tissues from age-matched wild type C57Bl/6 mice (Fig. S1D). The R3VE variant showed similar immunodetection to R3VQ on PS2APP mouse tissue (Fig. S1E).
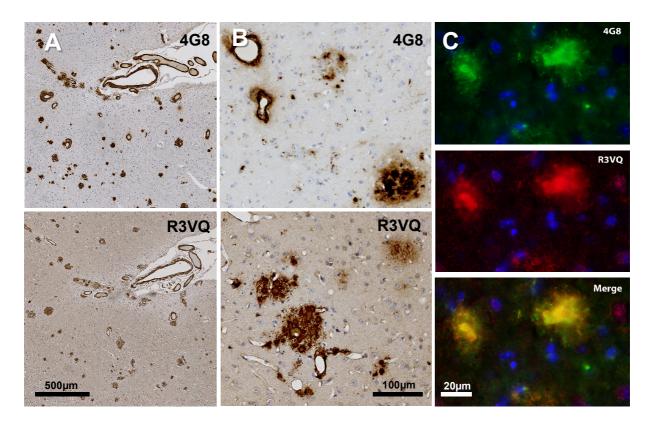
Fig. 2. Immunohistochemical characterization of VHH R3VQ as a specific probe for labeling of amyloid deposits.
R3VQ show similar sensitivity and selectivity to reference antibody 4G8 for detecting amyloid plaques and cerebral amyloid angiopathy (CAA) on both human AD (A) and PS2APP mouse (B) paraffin sections. Double immunofluorescent staining of 4G8 (green) and R3VQ (red) on brain tissue from a young PS2APP mouse confirmed the high specificity of R3VQ (C).

3.2. In vivo labeling of Aβ-positive lesions

3.2.1. Diffusion of R3VQ after stereotaxic brain injection

To test the ability of R3VQ to diffuse in the brain and to label *in vivo* amyloid plaques, six micrograms of R3VQ was stereotaxically injected into the cortex of 12-month old PS2APP mice (n=2). The mice were sacrificed 2 hours after injection. IHC revealed that R3VQ diffused in a large spherical region (approximatively 3 mm diameter) and amyloid plaques were detected in this volume (Fig. S2A). The results demonstrate a good ability of R3VQ to diffuse through living tissue and to label Aβ lesions quite rapidly (< 2 hours). To summarize, the VHH R3VQ was able to diffuse in the brain and specifically target amyloid plaques *in vivo*.

3.2.2. BBB transit and diffusion of R3VQ after intravenous injection

To investigate if R3VQ-S-AF488 crossed the BBB, a 50-mg/kg dose was injected iv into two 12-month-old PS2APP mice. In parallel, two age-matched PS2APP were injected with PBS (negative controls) or with AlexaFluor 488 conjugated anti-Aβ mAb 4G8 (4G8-S-AF488; 50 mg/kg) as controls for BBB passage of standard immunoglobulins. Four hours after injection, the mice were sacrificed and paraffin brain sections were prepared. In R3VQ-S-AF488 injected mice immunostaining using anti-His mAb showed extensive plaque labeling throughout the brain. This demonstrates that the VHH conjugate was able to cross the BBB,

diffuse widely in the living brain and label its target. In contrast, no staining was found in mice injected with PBS (Fig. S3) and only few plaques in restricted brain regions were detected following 4G8-S-AF488 injections, underlining very limited BBB permeability for regular immunoglobulins (Fig. S3).

3.2.3. Real-time imaging of R3VQ after intravenous injection

A 50-mg/kg dose of R3VQ-S-AF488 was injected in the tail vein of a one-year-old PS2APP mouse. The conjugate extravasation and diffusion in the brain was recorded for 4 hours post injection using two-photon microscopy of a cortical brain window (from surface to 360 μm deep). Fig. 3A displays *in vivo* imaging of the same region of interest at 1 and 30 min post-injection of R3VQ-S-AF488. A few seconds after iv injection, strong labeling of arborescent vessels was observed. After 20 min only few capillary vessels were still labeled. This suggested a short half-life (10-20 min) of conjugated VHH in the blood circulation [29]. Shortly after injection a green fluorescent "cloud" formed and spread in the parenchymal space, reminiscent of the diffusion observed following stereotaxic injection of R3VQ (Fig. S2A). Thirty minutes after injection, both amyloid plaques and vascular Aβ (CAA) began to be visualized. *In vivo* labeling of Aβ deposition in plaques and vessels remained up to four hours after injection (Fig. 3B and Video S1), suggesting a half-life of R3VQ-S-AF488 extending over several hours in the brain. Four hours after the intravenous injection of R3VQ-S-AF488, the brain was harvested and paraffin sections were prepared.

Using anti-His mAb, immunodetection of amyloid plaques by R3VQ-S-AF488 was observed throughout the entire brain with an accompanying background signal which could correspond to the diffusion halo of the VHH (Fig. 3C). Additional experiments were performed with a lower dose of R3VQ-S-AF488 (10 mg/kg) and *in vivo* detection of Aβ deposition was observed but with decreased intensity. These results demonstrated that R3VQ brain penetration and its ability to label brain Aβ lesions were dose-dependent, an observation which was also confirmed by IHC (Fig. 3D).
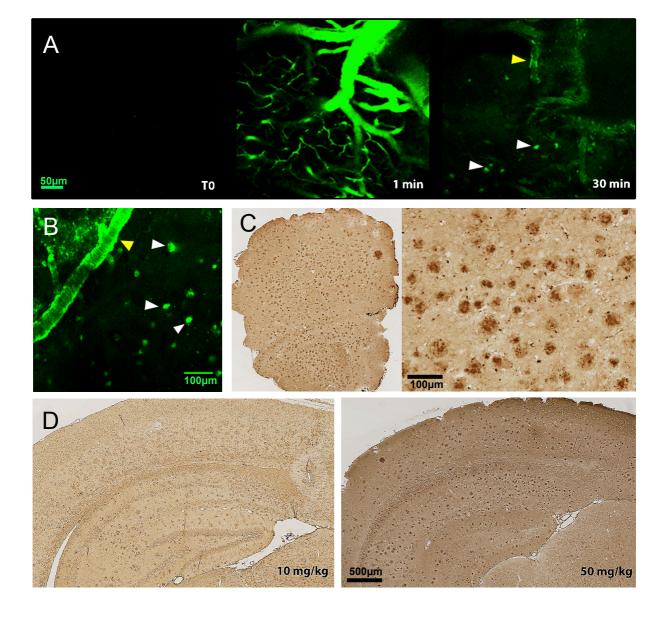
Fig. 3. In vivo imaging of VHH R3VQ-S-AF488 using two-photon microscopy.

(A, B) *In vivo* imaging in the brain after iv injection of R3VQ-S-AF488 in a one-year-old PS2APP mouse. Maximum intensity projection with a projected volume extending 360μm deep from the surface of the cortex. T0 represents the baseline imaging before iv injection. Yellow arrowheads indicate vascular Aβ and white arrowheads indicate parenchymal Aβ deposits. (B) was obtained four hours after injection. (C) *Ex vivo* detection of amyloid plaques in PS2APP mouse that received iv injection of R3VQ-S-AF488 four hours before sacrifice. Immunostaining of amyloid plaques by extrinsic R3VQ was observed throughout the brain. The right image showed a magnified view from the left image. (D) Comparison of immunostaining of amyloid plaques in PS2APP mice receiving iv injections of either 10 mg/kg or 50 mg/kg of R3VQ-S-AF488.

The basic pI of VHHs has been proposed to be an important parameter predicting their ability to transmigrate across the BBB [18]. R3VE-S-AF488 conjugate was prepared with a pI of ca. 7.5 (Fig. S4A, B). A 10 mg/kg dose of R3VE-S-AF488 was iv injected in a one-year-old PS2APP mouse. Forty-five minutes after injection, only cerebral amyloid angiopathy was

shown without signs of extravasation or labeling of amyloid plaques (Fig. S4C), supporting the hypothesis that the positive charges present on the surface of VHHs play a critical role for brain penetration of these antibodies across the BBB.

Finally, R3VQ-S-AF488 at 50 mg/kg was intravenously injected in a wild-type mouse. Except for initial blood vessel labeling, no specific *in vivo* staining in the brain parenchyma was observed using two-photon microscopy imaging. A fluorescent cloud appeared 1 hour after injection (suggesting presence of unbound R3VQ-S-AF488 in the brain) but then rapidly vanished (Fig. S5). These data indicate that R3VQ-S-AF488 crosses the BBB in wild-type mice but is not retained in the absence of amyloid plaques.

In summary, using two-photon microscopy after intravenous injection of R3VQ-S-AF488, we demonstrated the ability of the VHH R3VQ to cross the BBB, to reach its extracellular cerebral target and to transport fluorescent probes across the BBB, allowing its real-time visualization.

3.3. Selection and characterization of a VHH recognizing intracellular targets

3.3.1. Generation and engineering of A2

One alpaca was immunized with AD phospho-tau (pTau) enriched brain extracts and a second alpaca was immunized with a mono-phosphorylated peptide derived from the C-terminus of the tau protein (pS422 peptide) coupled to the KLH protein. The sera of immunized alpacas recognized both pTau and non-phosphorylated tau. The immunized animals generated 2 phage-VHH libraries of about 3×10^8 clones each. In order to expand the diversity of VHHs, a pooled library from these two animals was used for panning experiments by Phage Display. After 3 panning cycles with pTau protein, one clone was found to bind specifically to pTau and was referred to as A2. C-terminally His tagged A2 was produced as described above for R3VQ VHH (yield 5 mg/l of culture). Only one band was observed by SDS-PAGE (Fig. 4A). Analysis by IEF-NEPHGE showed that the pI of A2 was higher than 9.5 (Fig. 4B). ELISA was performed on pTau and pS422 peptide coupled to ovalbumin. pTau corresponded to the full-length tau protein phosphorylated at multiple sites including S422. A2 bound to both full-length pTau protein and the pS422-containing peptide. Lack of binding to non-phosphorylated-tau demonstrated that A2 was specific for a phosphorylated epitope (Fig. 4C).

For the purpose of *in vivo* analysis, an A2-SH variant was prepared and conjugated to AF488 as previously described for R3VQ-S-AF488 (see above). The pI of A2-SH and A2-S-AF488 was between 9.5 and 10.7. The addition of maleimido-AF488 to A2-SH slightly decreased the pI of A2-SH as already observed with R3VQ-S-AF488 (Fig. 4B).
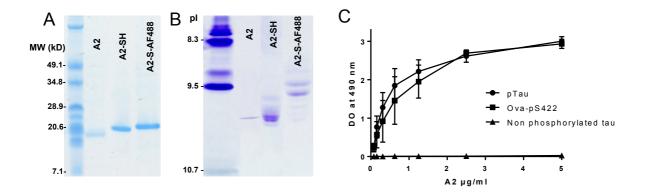
Fig. 4. Biochemical characterization of VHH A2 and its variants.

(A) Protein analysis of VHH A2, A2-SH and A2-S-AF488 by SDS-PAGE. (B) Determination of pI of A2 variants by NEPHGE on 3-10 IEF gel. (C) Binding of A2 to phospho-tau (pTau), non-phosphorylated tau and Ova-pS422 peptide.

3.3.2. Immunodetection of tau brain lesions in mice and in human brain sections

VHH A2 allowed detection of intracellular neurofibrillary tangle-like structures in Tg4510 mouse brain tissues using paraffin sections with or without any antigen retrieval pretreatment (Fig. 5B). Specific staining of neurofibrillary tau inclusions with A2 was also readily obtained on free floating sections from Tg4510 mice (Fig. S6A). Comparable staining was observed using the reference anti-pTau AT8 mAb [30]. No labeling was noted with tissues from age-matched wild type mice (Fig. S6A). Double labeling performed on mouse sections using the A2 and reference antibody AT8 showed strong colocalization of the two immunostainings (Fig. 5C). The load of tau lesions detected by A2 and AT8 antibodies were highly correlated underlining similar sensitivity-specificity profiles (Fig. S6B).

Using paraffin-fixed AD brain sections, VHH A2 detected neurofibrillary tau tangles in neuronal soma, tortuous fibers and dystrophic neurites was also obtained in (Fig. 5A). Additional experiments (Fig. S7) showed that VHH A2 also recognized tau-positive lesions from other tauopathies e.g. glial inclusions in tissues from patients with fronto-temporal dementia (oligodendroglial coiled bodies) or with progressive supranuclear palsy (astrocytic tufts).

To our knowledge, this is the first VHH that has been shown to detect tau lesions in both tau transgenic mouse and human tauopathy brain tissues.
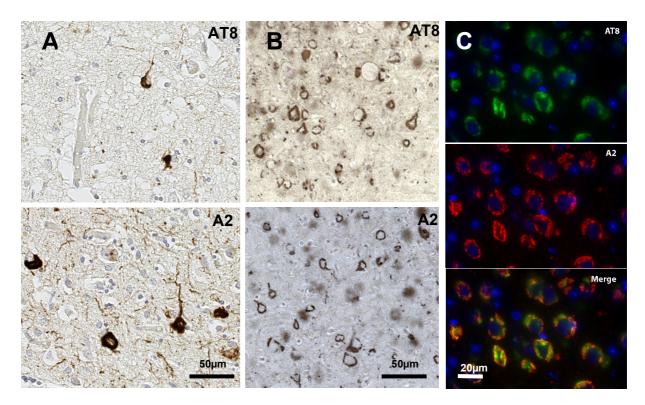
Fig. 5. Immunohistochemical characterization of VHH A2 as a specific probe for labeling neurofibrillary tangles.

A2 shows similar sensitivity and selectivity to AT8 in detecting NFTs on both human AD (A) and Tg4510 mouse (B) brain sections. Double immunofluorescence staining of AT8 and A2 on Tg4510 mouse tissue confirmed the high specificity of A2 (C).

3.4. In vivo labeling of tau-positive lesions:

3.4.1. Diffusion of A2 after stereotaxic brain injection

To test the ability of A2 to immunolabel tau lesions *in vivo*, A2 was stereotaxically injected into the cortex of 10-month-old Tg4510 mice. The mice were sacrificed 2 hours after injection. IHC revealed that A2 had diffused throughout the entire brain and bound to pTau aggregates in numerous cortical and subcortical regions (Fig. S2B).

3.4.2. BBB transit and diffusion of A2 after intravenous injection

To investigate if A2-S-AF488 crosses the BBB, the same systematic approach as implemented for R3VQ-S-AF488 (see above) was applied. A 10 mg/kg dose of A2-S-AF488 was injected iv in two 8-month-old Tg4510 mice that were sacrificed 4 hours later. Immunostaining using anti-A2 polyclonal antibody showed binding to a large number of NFT-like structures in the brain, demonstrating that A2-S-AF488 crossed the BBB, diffused extensively throughout the brain *in vivo* and labeled pTau aggregates. By contrast, no staining was found in the mice injected with PBS or with a conventional antibody specific for pTau (Fig. S3).

3.4.3. Real-time imaging A2 after intravenous injection

VHH A2-S-AF488 (10 mg/kg) was injected in the tail vein of Tg4510 mice. A2-S-AF488 extravasation and diffusion in the brain was monitored for 4 hours post injection using two-

photon microscopy imaging of the cortical surface up to 350 µm deep. Immediately after iv injection, cerebral blood vessels showed strong fluorescence, as observed for R3VQ. Identification of NFT-like structures was possible 2 hours after injection (Fig. 6A). A persistent and specific labeling of NFTs was observed even 4 hours after injection (Fig. 6B) and the 3D reconstruction of the immuno-detected objects revealed the standard flame-shaped morphology of tangles (Video S2). Four hours after injection, the mice were sacrificed, immunohistochemistry was performed using anti-A2 polyclonal antibody to demonstrate the presence of A2-S-AF488 in the brain. Extensive tau immunostaining throughout the brain was also confirmed in postmortem tissue (Fig. 6C).
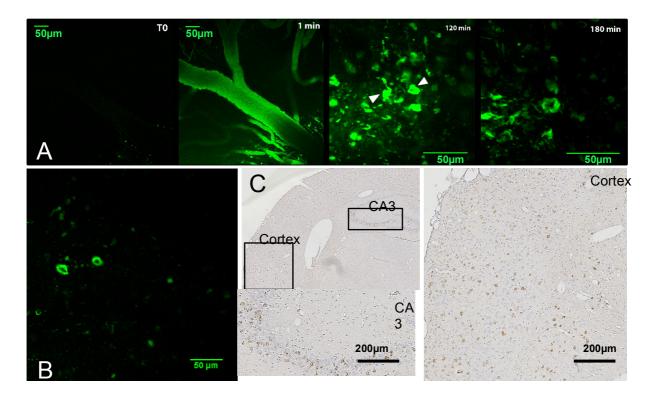

Fig. 6. In vivo imaging of VHH A2-S-AF488 using two-photon microscopy.

(A) Maximum intensity projection of fluorescence in an 8-month-old Tg4510 mouse at different timepoints after iv injection of A2-S-AF488 at 10 mg/kg. Whereas only faint non-specific signal could be detected before iv injection (T0), a strong staining of arborescent vessels was observed a few seconds after iv injection. Specific labeling of NFTs (white arrows) occurred only after 120 min, with a maximum intensity after 180 min. (B) Specific staining of NFTs was observed 4 hours post injection. (C) *Ex vivo* detection of NFT labeling by extrinsic A2 VHH on brain sections obtained from Tg4510 mice four hours after iv injection of A2-S-AF488. The image on the bottom left and the image on the right showed magnified views in the cortex and CA3.

In summary, VHH A2-S-AF488 efficiently crossed the BBB and penetrated into neurons to reach its cytoplasmic target. As for *in vivo* R3VQ experiments, target labeling was visible four hours after administration demonstrating slow turnover of target-associated VHHs in the brain.

4. DISCUSSION

4.1. VHHs bind to both extracellular and intracellular brain targets

VHHs were generated to Aβ42 and phospho-tau (R3VQ and A2, respectively). Their specificities were biochemically assessed and then confirmed by immunohistochemistry on both human and AD transgenic mouse brain tissues. To the best of our knowledge, the VHH A2 presented here is the first engineered VHH capable of immunodetecting AD-associated intraneuronal NFT pathology.

By means of stereotaxic injection we then confirmed the ability of R3VQ and A2 to label their targets *in vivo* after rapid diffusion in brain tissue, a result that may be explained by the small size of the constructs [13]. Notably, the antigen binding properties of both VHHs were preserved after conjugation with AlexaFluor 488, therefore opening up opportunities to use labeled VHHs for *in vivo* imaging.

4.2. VHHs cross the BBB and efficiently diffuse in the brain

A few VHHs have been shown to cross the BBB by receptor-mediated transcytosis [31,32]. We have previously shown that VHH E9 with basic pI was able to passively cross the BBB, diffuse in the brain parenchyma and label astrocytes *in vivo* [18].

An anti-Aβ VHH (pa2H) was previously reported to cross the BBB *in vivo* [29]. However pa2H brain uptake was too low to allow *in vivo* imaging. More recently the same research group designed a glutathione PEGylated liposomal encapsulation system to enhance the delivery of pa2H across the BBB [33]. SPECT imaging performed in this study did not however allow the visualization of pa2H brain penetration. In our study plaques and NFTs were detected *in vivo* after a single iv injection of fluorescent R3VQ and A2 respectively, confirming they readily cross the BBB and have exquisite sensitivity of the engineered VHHs. The presence of VHHs throughout the brain was subsequently confirmed by immunohistochemistry. Labeling of amyloid plaques and NFTs by R3VQ and A2 respectively was detectable with high signal intensity up to 4 hours post-injection, suggesting a long half-life of VHHs in the brain, at least when bound to target. Indeed, Nabuurs and collaborators indicated that their anti-Aβ VHH remained detectable in the brain for at least 24 hours post-injection [29].

R3VQ-S-AF488 demonstrated rapid diffusion (0.5-1 h post-injection) throughout the brain of PS2APP mice and showed high specificity for Aβ deposits in both parenchymal (Aβ plaques) and vascular spaces (CAA). In the Tg4510 mice receiving iv injection of A2-S-AF488, the specific staining of NFTs was observed 2h post-injection, much later than with R3VQ-S-AF488, probably because A2-S-AF488 had to cross two barriers: the BBB and the cell membrane of neurons containing NFTs.

Traumatic uncontrolled BBB opening during the two-photon imaging procedure related to local brain bleeding due to craniotomy could have explained our results, however such a possibility is implausible. First we observed that both R3VQ and A2 VHHs were distributed throughout the whole brain following iv injection and not only in the vicinity of the cranial window as would be the case if there was local bleeding. Second, four hours after iv injection into transgenic mice *without any cranial surgery* both fluorescent VHHs labeled their respective targets in the brain.

It remains possible that the passage of VHHs across the BBB resulted from a "naturally-compromised" barrier in the transgenic mice. Indeed, during normal aging, the permeability of the BBB increases, and disruption of the BBB occurs in a number of neurological disorders,

including AD [34,35]. A recent study indicates however a lack of BBB permeability in the PS2APP transgenic line we used for R3VQ imaging [36], even at the oldest ages. Evidence of BBB leakage has been reported in Tg4510 mice but starting at 9 months of age [37] however we conducted *in vivo* imaging in younger animals. We confirmed the absence of BBB leakage in the two models we used by demonstrating that conventional immunoglobulin specific for the targeted antigens did not significantly penetrate into the CNS following iv injection. Finally, it could be argued that high VHH concentrations (from 10 to 50 mg/kg) induce a transient disruption of the BBB and an extravasation of the VHH. However, our previous study using an Evans Blue dye exclusion assay showed that VHHs do not compromise the BBB even using VHH at very high concentration (133 mg/kg, *i.e.* 4 mg for an adult mouse) [18].

To summarize we showed that both R3VQ and A2 can cross the BBB after peripheral administration and bind to extracellular (plaques) and intracellular (tangles) brain targets. The factors influencing VHH transit across the BBB are poorly understood. The molecular size of VHHs was demonstrated to be an important parameter for their brain penetration with a rate of passage decreased for large-sized VHH constructs: dimers of VHH (molecular weight of 28kDa) or a VHH fused to EGFP (molecular weight of 40 kDa) [18]. The molecular weight of the VHH-S-AF488 used in the present study was slightly increased by the addition of a fluorophore (+ 1 kDa), but this modification did not affect their apparent brain penetration. Basic pI also appears to be an important parameter since a VHH variant with a near-neutral pI (R3VE) showed only limited brain penetration. In our previous study using an anti-GFAP VHH we showed that BBB crossing was not energy-dependent, suggesting active transport is not involved [18]. The transmigration of basic VHHs through the BBB probably occurs by adsorptive-mediated endocytosis initiated by non-specific, charge-based interactions with proteins at the endothelial cell surface [38–41]. Recent studies demonstrated that proteins with high net positive charge have indeed the ability to penetrate mammalian cells and deliver macromolecules into cells *in vitro* and *in vivo* [42,43]. Understanding the precise mechanism of VHH BBB passage will be important for optimizing efficient targeted probes in the future.

4.3.   VHH potential for AD diagnosis

Until now the development of imaging markers for AD brain lesions has focused on PET ligands [44–50]. However PET imaging suffers from numerous drawbacks, namely, low spatial resolution, exposure to radiation, limited availability and high cost. Conversely, MRI provides information with high spatial resolution, does not rely on ionizing radiations and is widely available for clinical use. Previous attempts have been made to use MR contrast agents for visualizing amyloid deposits in AD mouse models. However these studies relied on artificial BBB opening by ultrasound [7,8] or BBB permeability enhancers such as mannitol [9]. With the goal of developing a more physiological approach we are currently improving a method for site-specifically conjugating VHHs to paramagnetic gadolinium. The VHHs described in the present work could be conjugated with gadolinium to provide a novel MR imaging agents for AD.

An important parameter to consider is the potential immunogenicity of VHHs in human patients, if they would be applied for diagnosis and/or follow-up of the patients with AD. VHHs actually have multiple advantages for diagnostic applications, such as small size, high stability, fast blood clearance [12]. Also VHH sequences share high homology with human VH

sequences[51]. All these characteristics predict low immunogenicity of VHHs. Indeed, previous studies underlined that VHHs did not induce an immunogenic reaction after injection in mice [52–54] and a lower risk of immunogenicity was expected in humans. Moreover, VHHs can be humanized without loss of their stability, affinity and specificity [55,56], and numerous VHHs are currently in clinical development (http://www.ablynx.com/rd-portfolio/overview/).

4.4. Conclusions

We describe novel VHHs that could be potentially used as *in vivo* imaging agents able to detect brain lesions observed in human diseases, e.g. Alzheimer's disease. VHH R3VQ binds to brain Aβ deposits and VHH A2 recognizes neuronal pathological tau inclusions. VHHs are able to penetrate the brain more efficiently than conventional IgGs and they can be readily site-specifically modified for *in vivo* imaging of neurodegenerative diseases with extracellular or intracellular misfolded protein aggregates.

Acknowledgments

References

[1]   M.J. Coloma, H.J. Lee, A. Kurihara, E.M. Landaw, R.J. Boado, S.L. Morrison, W.M. Pardridge, Transport across the primate blood-brain barrier of a genetically engineered chimeric monoclonal antibody to the human insulin receptor., Pharm. Res. 17 (2000) 266–74. doi:10.1023/A:1007592720793.

[2]   F. Bard, C. Cannon, R. Barbour, R.L. Burke, D. Games, H. Grajeda, T. Guido, K. Hu, J. Huang, K. Johnson-Wood, K. Khan, D. Kholodenko, M. Lee, I. Lieberburg, R. Motter, M. Nguyen, F. Soriano, N. Vasquez, K. Weiss, B. Welch, P. Seubert, D. Schenk, T. Yednock, Peripherally administered antibodies against amyloid beta-peptide enter the central nervous system and reduce pathology in a mouse model of Alzheimer disease., Nat. Med. 6 (2000) 916–9. doi:10.1038/78682.

[3]   J. Niewoehner, B. Bohrmann, L. Collin, E. Urich, H. Sade, P. Maier, P. Rueger, J.O. Stracke, W. Lau, A.C. Tissot, H. Loetscher, A. Ghosh, P.-O. Freskgård, Increased brain penetration and potency of a therapeutic antibody using a monovalent molecular shuttle., Neuron. 81 (2014) 49–60. doi:10.1016/j.neuron.2013.10.061.

[4]   R.J. Boado, E.K.-W. Hui, J.Z. Lu, R.K. Sumbria, W.M. Pardridge, Blood-brain barrier molecular trojan horse enables imaging of brain uptake of radioiodinated recombinant protein in the rhesus monkey., Bioconjug. Chem. 24 (2013) 1741–9. doi:10.1021/bc400319d.

[5]   J. a. Couch, Y.J. Yu, Y. Zhang, J.M. Tarrant, R.N. Fuji, W.J. Meilandt, H. Solanoy, R.K. Tong, K. Hoyte, W. Luk, Y. Lu, K. Gadkar, S. Prabhu, B. a. Ordonia, Q. Nguyen, Y. Lin, Z. Lin, M. Balazs, K. Scearce-Levie, J. a. Ernst, M.S. Dennis, R.J. Watts, Addressing Safety Liabilities of TfR Bispecific Antibodies That Cross the Blood-Brain Barrier, Sci. Transl. Med. 5 (2013) 183ra57–183ra57. doi:10.1126/scitranslmed.3005338.

[6]   S. Ohshima-Hosoyama, H. a Simmons, N. Goecks, V. Joers, C.R. Swanson, V. Bondarenko, R. Velotta, K. Brunner, L.D. Wood, R.H. Hruban, M.E. Emborg, A monoclonal antibody-GDNF fusion protein is not neuroprotective and is associated with proliferative pancreatic lesions in parkinsonian monkeys., PLoS One. 7 (2012) e39036. doi:10.1371/journal.pone.0039036.

[7]   M.D. Santin, T. Debeir, S.L. Bridal, T. Rooney, M. Dhenain, Fast in vivo imaging of amyloid plaques using μ-MRI Gd-staining combined with ultrasound-induced blood-brain barrier opening., Neuroimage. 79 (2013) 288–94. doi:10.1016/j.neuroimage.2013.04.106.

[8]   B. Matharu, N. Spencer, F. Howe, B. Austen, Gadolinium-complexed Aβ-binding contrast agents for MRI diagnosis of Alzheimer's Disease., Neuropeptides. (2015) 1–8. doi:10.1016/j.npep.2015.07.001.

[9]   E.M. Sigurdsson, Y.Z. Wadghiri, L. Mosconi, J. a. Blind, E. Knudsen, A. Asuni, H. Scholtzova, W.H. Tsui, Y. Li, M. Sadowski, D.H. Turnbull, M.J. de Leon, T. Wisniewski, A non-toxic ligand for voxel-based MRI analysis of plaques in AD transgenic mice, Neurobiol. Aging. 29 (2008) 836–847. doi:10.1016/j.neurobiolaging.2006.12.018.

[10]   A. Rodriguez, S.B. Tatter, W. Debinski, Neurosurgical Techniques for Disruption of the Blood-Brain Barrier for Glioblastoma Treatment., Pharmaceutics. 7 (2015) 175–87. doi:10.3390/pharmaceutics7030175.

[11]   C. Hamers-Casterman, T. Atarhouch, S. Muyldermans, G. Robinson, C. Hamers, E.B. Songa, N. Bendahman, R. Hamers, Naturally occurring antibodies devoid of light chains., Nature. 363 (1993) 446–8. doi:10.1038/363446a0.

[12]   S. Muyldermans, Nanobodies: natural single-domain antibodies., Annu. Rev. Biochem.

82 (2013) 775–97. doi:10.1146/annurev-biochem-063011-092449.

[13]   C. Perruchini, F. Pecorari, J.-P. Bourgeois, C. Duyckaerts, F. Rougeon, P. Lafaye, Llama VHH antibody fragments against GFAP: better diffusion in fixed tissues than classical monoclonal antibodies., Acta Neuropathol. 118 (2009) 685–95. doi:10.1007/s00401-009-0572-6.

[14]   V. Cortez-Retamozo, M. Lauwereys, G. Hassanzadeh Gh, M. Gobert, K. Conrath, S. Muyldermans, P. De Baetselier, H. Revets, Efficient tumor targeting by single-domain antibody fragments of camels., Int. J. Cancer. 98 (2002) 456–62. doi:10.1002/ijc.10212.

[15]   Z. Li, B.-F. Krippendorff, S. Sharma, A.C. Walz, T. Lavé, D.K. Shah, Influence of molecular size on tissue distribution of antibody fragments., MAbs. 8 (2016) 113–9. doi:10.1080/19420862.2015.1111497.

[16]   U. Rothbauer, K. Zolghadr, S. Tillib, D. Nowak, L. Schermelleh, A. Gahl, N. Backmann, K. Conrath, S. Muyldermans, M.C. Cardoso, H. Leonhardt, Targeting and tracing antigens in live cells with fluorescent nanobodies., Nat. Methods. 3 (2006) 887–9. doi:10.1038/nmeth953.

[17]   J. Helma, K. Schmidthals, V. Lux, S. Nüske, A.M. Scholz, H.-G. Kräusslich, U. Rothbauer, H. Leonhardt, Direct and dynamic detection of HIV-1 in living cells., PLoS One. 7 (2012) e50026. doi:10.1371/journal.pone.0050026.

[18]   T. Li, J.-P. Bourgeois, S. Celli, F. Glacial, A.-M. Le Sourd, S. Mecheri, B. Weksler, I. Romero, P.-O. Couraud, F. Rougeon, P. Lafaye, Cell-penetrating anti-GFAP VHH and corresponding fluorescent fusion protein VHH-GFP spontaneously cross the blood-brain barrier and specifically recognize astrocytes: application to brain imaging., FASEB J. 26 (2012) 3969–79. doi:10.1096/fj.11-201384.

[19]   I. Van Audenhove, K. Van Impe, D. Ruano-Gallego, S. De Clercq, K. De Muynck, B. Vanloo, H. Verstraete, L.Á. Fernández, J. Gettemans, Mapping cytoskeletal protein function in cells by means of nanobodies., Cytoskeleton (Hoboken). 70 (2013) 604–22. doi:10.1002/cm.21122.

[20]   A. Rocchetti, C. Hawes, V. Kriechbaumer, Fluorescent labelling of the actin cytoskeleton in plants using a cameloid antibody., Plant Methods. 10 (2014) 12. doi:10.1186/1746-4811-10-12.

[21]   B. Traenkle, F. Emele, R. Anton, O. Poetz, R.S. Haeussler, J. Maier, P.D. Kaiser, A.M. Scholz, S. Nueske, A. Buchfellner, T. Romer, U. Rothbauer, Monitoring interactions and dynamics of endogenous beta-catenin with intracellular nanobodies in living cells., Mol. Cell. Proteomics. 14 (2015) 707–23. doi:10.1074/mcp.M114.044016.

[22]   J. Maier, B. Traenkle, U. Rothbauer, Real-time analysis of epithelial-mesenchymal transition using fluorescent single-domain antibodies., Sci. Rep. 5 (2015) 13402. doi:10.1038/srep13402.

[23]   P. Lafaye, I. Achour, P. England, C. Duyckaerts, F. Rougeon, Single-domain antibodies recognize selectively small oligomeric forms of amyloid beta, prevent Abeta-induced neurotoxicity and inhibit fibril formation., Mol. Immunol. 46 (2009) 695–704. doi:10.1016/j.molimm.2008.09.008.

[24]   L. Ozmen, A. Albientz, C. Czech, H. Jacobsen, Expression of transgenic APP mRNA is the key determinant for beta-amyloid deposition in PS2APP transgenic mice., Neurodegener. Dis. 6 (2009) 29–36. doi:10.1159/000170884.

[25]   C. Weidensteiner, F. Metzger, A. Bruns, B. Bohrmann, B. Kuennecke, M. von Kienlin, Cortical hypoperfusion in the B6.PS2APP mouse model for Alzheimer's disease: comprehensive phenotyping of vascular and tissular parameters by MRI., Magn.

Reson. Med. 62 (2009) 35–45. doi:10.1002/mrm.21985.

[26]   K. Santacruz, J. Lewis, T. Spires, J. Paulson, L. Kotilinek, M. Ingelsson, a Guimaraes, M. DeTure, M. Ramsden, E. McGowan, C. Forster, M. Yue, J. Orne, C. Janus, a Mariash, M. Kuskowski, B. Hyman, M. Hutton, K.H. Ashe, Tau suppression in a neurodegenerative mouse model improves memory function., Science. 309 (2005) 476–81. doi:10.1126/science.1113694.

[27]   P. Agarwal, C.R. Bertozzi, Site-specific antibody-drug conjugates: the nexus of bioorthogonal chemistry, protein engineering, and drug development., Bioconjug. Chem. 26 (2015) 176–92. doi:10.1021/bc5004982.

[28]   I. Alafuzoff, D.R. Thal, T. Arzberger, N. Bogdanovic, S. Al-Sarraj, I. Bodi, S. Boluda, O. Bugiani, C. Duyckaerts, E. Gelpi, S. Gentleman, G. Giaccone, M. Graeber, T. Hortobagyi, R. Höftberger, P. Ince, J.W. Ironside, N. Kavantzas, A. King, P. Korkolopoulou, G.G. Kovács, D. Meyronet, C. Monoranu, T. Nilsson, P. Parchi, E. Patsouris, M. Pikkarainen, T. Revesz, A. Rozemuller, D. Seilhean, W. Schulz-Schaeffer, N. Streichenberger, S.B. Wharton, H. Kretzschmar, Assessment of beta-amyloid deposits in human brain: a study of the BrainNet Europe Consortium., Acta Neuropathol. 117 (2009) 309–20. doi:10.1007/s00401-009-0485-4.

[29]   R.J. a Nabuurs, K.S. Rutgers, M.M. Welling, A. Metaxas, M.E. de Backer, M. Rotman, B.J. Bacskai, M. a van Buchem, S.M. van der Maarel, L. van der Weerd, In vivo detection of amyloid-β deposits using heavy chain antibody fragments in a transgenic mouse model for Alzheimer's disease., PLoS One. 7 (2012) e38284. doi:10.1371/journal.pone.0038284.

[30]   M. Mercken, M. Vandermeeren, U. Lübke, J. Six, J. Boons, A. Van de Voorde, J.J. Martin, J. Gheuens, Monoclonal antibodies with selective specificity for Alzheimer Tau are directed against phosphatase-sensitive epitopes., Acta Neuropathol. 84 (1992) 265–72. http://www.ncbi.nlm.nih.gov/pubmed/1384266 (accessed December 18, 2013).

[31]   A. Muruganandam, J. Tanha, S. Narang, D. Stanimirovic, Selection of phage-displayed llama single-domain antibodies that transmigrate across human blood-brain barrier endothelium., FASEB J. 16 (2002) 240–2. doi:10.1096/fj.01-0343fje.

[32]   K.S. Rutgers, A. van Remoortere, M. a van Buchem, C.T. Verrips, S.M. Greenberg, B.J. Bacskai, M.P. Frosch, S.G. van Duinen, M.L. Maat-Schieman, S.M. van der Maarel, Differential recognition of vascular and parenchymal beta amyloid deposition., Neurobiol. Aging. 32 (2011) 1774–83. doi:10.1016/j.neurobiolaging.2009.11.012.

[33]   M. Rotman, M.M. Welling, A. Bunschoten, M.E. de Backer, J. Rip, R.J. a Nabuurs, P.J. Gaillard, M. a van Buchem, S.M. van der Maarel, L. van der Weerd, Enhanced glutathione PEGylated liposomal brain delivery of an anti-amyloid single domain antibody fragment in a mouse model for Alzheimer's disease., J. Control. Release. 203 (2015) 40–50. doi:10.1016/j.jconrel.2015.02.012.

[34]   M. a Erickson, W. a Banks, Blood-brain barrier dysfunction as a cause and consequence of Alzheimer's disease., J. Cereb. Blood Flow Metab. 33 (2013) 1500–13. doi:10.1038/jcbfm.2013.135.

[35]   F. Marques, J.C. Sousa, N. Sousa, J.A. Palha, Blood-brain-barriers in aging and in Alzheimer's disease., Mol. Neurodegener. 8 (2013) 38. doi:10.1186/1750-1326-8-38.

[36]   N. Bien-Ly, C.A. Boswell, S. Jeet, T.G. Beach, K. Hoyte, W. Luk, V. Shihadeh, S. Ulufatu, O. Foreman, Y. Lu, J. DeVoss, M. van der Brug, R.J. Watts, Lack of Widespread BBB Disruption in Alzheimer's Disease Models: Focus on Therapeutic Antibodies., Neuron.

88 (2015) 289–97. doi:10.1016/j.neuron.2015.09.036.

[37]   L.J. Blair, H.D. Frauen, B. Zhang, B. a Nordhues, S. Bijan, Y.-C. Lin, F. Zamudio, L.D. Hernandez, J.J. Sabbagh, M.-L.B. Selenica, C. a Dickey, Tau depletion prevents progressive blood-brain barrier damage in a mouse model of tauopathy., Acta Neuropathol. Commun. 3 (2015) 8. doi:10.1186/s40478-015-0186-2.

[38]   N.J. Abbott, Blood-brain barrier structure and function and the challenges for CNS drug delivery., J. Inherit. Metab. Dis. 36 (2013) 437–49. doi:10.1007/s10545-013-9608-0.

[39]   A. Abulrob, H. Sprong, P. Van Bergen en Henegouwen, D. Stanimirovic, The blood-brain barrier transmigrating single domain antibody: mechanisms of transport and antigenic epitopes in human brain endothelial cells., J. Neurochem. 95 (2005) 1201–14. doi:10.1111/j.1471-4159.2005.03463.x.

[40]   U. Bickel, T. Yoshikawa, W.M. Pardridge, Delivery of peptides and proteins through the blood-brain barrier., Adv. Drug Deliv. Rev. 46 (2001) 247–79. http://www.ncbi.nlm.nih.gov/pubmed/11259843.

[41]   a W. Vorbrodt, Ultracytochemical characterization of anionic sites in the wall of brain capillaries., J. Neurocytol. 18 (1989) 359–68. http://www.ncbi.nlm.nih.gov/pubmed/2746307.

[42]   J.J. Cronican, D.B. Thompson, K.T. Beier, B.R. McNaughton, C.L. Cepko, D.R. Liu, Potent delivery of functional proteins into Mammalian cells in vitro and in vivo using a supercharged protein., ACS Chem. Biol. 5 (2010) 747–52. doi:10.1021/cb1001153.

[43]   J.J. Cronican, K.T. Beier, T.N. Davis, J.-C. Tseng, W. Li, D.B. Thompson, A.F. Shih, E.M. May, C.L. Cepko, A.L. Kung, Q. Zhou, D.R. Liu, A class of human proteins that deliver functional proteins into mammalian cells in vitro and in vivo., Chem. Biol. 18 (2011) 833–8. doi:10.1016/j.chembiol.2011.07.003.

[44]   C.M. Clark, J. a Schneider, B.J. Bedell, T.G. Beach, W.B. Bilker, M. a Mintun, M.J. Pontecorvo, F. Hefti, A.P. Carpenter, M.L. Flitter, M.J. Krautkramer, H.F. Kung, R.E. Coleman, P.M. Doraiswamy, A.S. Fleisher, M.N. Sabbagh, C.H. Sadowsky, E.P. Reiman, P.E.M. Reiman, S.P. Zehntner, D.M. Skovronsky, Use of florbetapir-PET for imaging beta-amyloid pathology., JAMA. 305 (2011) 275–83. doi:10.1001/jama.2010.2008.

[45]   Y. Kimura, M. Ichise, H. Ito, H. Shimada, Y. Ikoma, C. Seki, H. Takano, S. Kitamura, H. Shinotoh, K. Kawamura, M.-R. Zhang, N. Sahara, T. Suhara, M. Higuchi, PET Quantification of Tau Pathology in Human Brain with 11C-PBB3., J. Nucl. Med. 56 (2015) 1359–65. doi:10.2967/jnumed.115.160127.

[46]   W.E. Klunk, H. Engler, A. Nordberg, Y. Wang, G. Blomqvist, D.P. Holt, M. Bergström, I. Savitcheva, G. Huang, S. Estrada, B. Ausén, M.L. Debnath, J. Barletta, J.C. Price, J. Sandell, B.J. Lopresti, A. Wall, P. Koivisto, G. Antoni, C.A. Mathis, B. Långström, Imaging brain amyloid in Alzheimer's disease with Pittsburgh Compound-B., Ann. Neurol. 55 (2004) 306–19. doi:10.1002/ana.20009.

[47]   M. Maruyama, H. Shimada, T. Suhara, H. Shinotoh, B. Ji, J. Maeda, M.-R. Zhang, J.Q. Trojanowski, V.M.-Y. Lee, M. Ono, K. Masamoto, H. Takano, N. Sahara, N. Iwata, N. Okamura, S. Furumoto, Y. Kudo, Q. Chang, T.C. Saido, A. Takashima, J. Lewis, M.-K. Jang, I. Aoki, H. Ito, M. Higuchi, Imaging of tau pathology in a tauopathy mouse model and in Alzheimer patients compared to normal controls., Neuron. 79 (2013) 1094–108. doi:10.1016/j.neuron.2013.07.037.

[48]   N. Okamura, S. Furumoto, M.T. Fodero-Tavoletti, R.S. Mulligan, R. Harada, P. Yates, S. Pejoska, Y. Kudo, C.L. Masters, K. Yanai, C.C. Rowe, V.L. Villemagne, Non-invasive

assessment of Alzheimer's disease neurofibrillary pathology using 18F-THK5105 PET., Brain. 137 (2014) 1762–71. doi:10.1093/brain/awu064.

[49] M. Brendel, A. Jaworska, F. Probst, F. Overhoff, V. Korzhova, S. Lindner, J. Carlsen, P. Bartenstein, R. Harada, Y. Kudo, C. Haass, F. van Leuven, N. Okamura, J. Herms, A. Rominger, microPET Imaging of Tau Pathology with [18F]-THK5117 in two Transgenic Mouse Models., J. Nucl. Med. 49 (2016) 1–32. doi:10.2967/jnumed.115.163493.

[50] D. Sehlin, X.T. Fang, L. Cato, G. Antoni, L. Lannfelt, S. Syvänen, Antibody-based PET imaging of amyloid beta in mouse models of Alzheimer's disease., Nat. Commun. 7 (2016) 10759. doi:10.1038/ncomms10759.

[51] I. Achour, P. Cavelier, M. Tichit, C. Bouchier, P. Lafaye, F. Rougeon, Tetrameric and homodimeric camelid IgGs originate from the same IgH locus., J. Immunol. 181 (2008) 2001–9. http://www.ncbi.nlm.nih.gov/pubmed/18641337.

[52] T.N. Baral, S. Magez, B. Stijlemans, K. Conrath, B. Vanhollebeke, E. Pays, S. Muyldermans, P. De Baetselier, Experimental therapy of African trypanosomiasis with a nanobody-conjugated human trypanolytic factor., Nat. Med. 12 (2006) 580–4. doi:10.1038/nm1395.

[53] K. Coppieters, T. Dreier, K. Silence, H. de Haard, M. Lauwereys, P. Casteels, E. Beirnaert, H. Jonckheere, C. Van de Wiele, L. Staelens, J. Hostens, H. Revets, E. Remaut, D. Elewaut, P. Rottiers, Formatted anti-tumor necrosis factor alpha VHH proteins derived from camelids show superior potency and targeting to inflamed joints in a murine model of collagen-induced arthritis., Arthritis Rheum. 54 (2006) 1856–66. doi:10.1002/art.21827.

[54] V. Cortez-Retamozo, N. Backmann, P.D. Senter, U. Wernery, P. De Baetselier, S. Muyldermans, H. Revets, Efficient cancer therapy with a nanobody-based conjugate., Cancer Res. 64 (2004) 2853–7. http://www.ncbi.nlm.nih.gov/pubmed/15087403 (accessed January 10, 2014).

[55] C. Vincke, R. Loris, D. Saerens, S. Martinez-Rodriguez, S. Muyldermans, K. Conrath, General strategy to humanize a camelid single-domain antibody and identification of a universal humanized nanobody scaffold., J. Biol. Chem. 284 (2009) 3273–84. doi:10.1074/jbc.M806889200.

[56] J.D. Unciti-Broceta, T. Del Castillo, M. Soriano, S. Magez, J. a Garcia-Salcedo, Novel therapy based on camelid nanobodies., Ther. Deliv. 4 (2013) 1321–36. doi:10.4155/tde.13.87.